24/12/2024 15:06

(Article begins on next page)

The Potential of Statistical RANS to Predict Knock Tendency: Comparison with LES and Experiments on a Spark-Ignition Engine

Abstract

Pollutant regulations and fuel consumption concerns are the driving guidelines for increased thermal efficiency and specific power in current internal combustion engines. The achievement of such challenging tasks in Spark Ignition units is often limited by the onset of knock, which hinders the possibility to operate the engine with the optimal combustion phasing. The sporadic occurrence of individual knocking events is related to cycle-to-cycle variability of turbulent combustion. This is avoidable by only accepting a safety margin from its earliest onset.

On one side, the stochastic nature of knock and turbulence-related combustion variability would indicate Large-Eddy Simulation (LES) as the most appropriate technique for CFD analyses. Nevertheless, Large-Eddy Simulation remains a very time- and CPU-demanding approach, hardly integrated in the industrial timeframe for the design exploration and development of new units. Therefore, Reynolds Averaged Navier Stokes (RANS) models representing the average flow are chosen to limit CPU and development times, though they suffer from the intrinsic inability to account for cycle-dependent phenomena (e.g. knock). This is particularly critical at knock-borderline conditions, where far-from-average knocking events may occur. A previously developed statistical RANS-PDF knock model partly overcomes this limitation using equations for mixture fraction and enthalpy variance, ultimately reconstructing log-normal distributions of knock intensity. This allows RANS simulations to be directly compared to the usual statistical knock analysis at the test-bench.

In this paper all the mentioned modelling techniques (LES, RANS and RANS-PDF) are applied to simulate combustion and knock in a currently made turbocharged GDI engine under knock-safe, knock-limited and light-knocking conditions. The study relevance lays in the critical comparison of the results. The full potential of the statistical RANS-PDF model for engine development is highlighted on a coherent basis. The possibility to preserve the RANS formalism while enriching the results with knock statistical description is a relevant advancement in the virtual design of high-efficiency engines.

Keywords: Cycle-to-Cycle Variability; Large-Eddy Simulation; statistical RANS; combustion; auto-ignition; knock intensity

1. Introduction

The recent trend in internal combustion engine (ICEs) design is predominantly driven by environmental and energy concerns regarding fuel consumption and engine-out pollution. The need to cut tailpipe emissions (e.g. Soot, CO, NO_x, and UHC) and the increasingly stringent regulations in terms of CO_2 are pushing engine manufacturers towards Spark Ignition (SI) units, for which such strict regulations are potentially easier to meet with respect to Compression Ignition (CI) engines using the three-way catalytic converter. However, the higher CO_2 emissions (compared to CI engines) and the restrictions on ultra-low NOx and PN also for the lean-burn GDI units will pose remarkable challenges for SI units to keep the pace with the ever-present evolution of CI engines [1]. Innovative injection and combustion strategies for both SI (e.g. pre-chamber systems, lean burn, ion current for knock detection) and CI (e.g. advanced piezo injection system and low swirl intake ports [2], reactivity-controlled combustion) architectures are expected to further increase the brake thermal efficiency for passenger vehicles. The International Energy Agency (IEA) [3] projects a continuous increase of the use of refined petroleum and other liquid fuels in the transportation field through 2040. In this context, gasoline and biofuel additives are expected to remain the primary transportation fuels with a 36% share of the energy use. The quest for lower fuel consumption and CO_2 reduction is pursued by developing ultra-efficient SI engines, avoiding the thermodynamics conditions leading to auto-ignition reviewed by Wang et al. [4] and measured by Zhen et al. [5]. Promising strategies fulfilling the mentioned targets are the "downsizing" and "down-speeding", i.e. a progressive reduction of the displaced volume and operating speed. In order to preserve the low-load/low-rpm performance for improved efficiency, the specific engine output needs to be increased through higher intake boosting and compression ratio. Both these design guidelines promote the conditions for knock onset, which constitutes the

major barrier for further developments of SI units [6]. This is critical in small downsized engines [7], and the reduction of such harmful events can be carried out through the optimization of intake air flow rate and charge motion [8].

Engine knock is induced by the auto-ignition (AI) of a portion of the end-gases ahead the propagating spark-ignited flame front [9]. At Knock Onset (KO) a local and quasi-instantaneous heat release produces a rapid and localized pressure rise in the combustion chamber. Based on Knock Intensity (KI) metrics, engine knock can be classified as light, heavy or super knock. Despite the lack of a unified description, even light knock usually exhibits pressure oscillations whose amplitude is in the range of 10 bar. This is not tolerated in ICEs as it leads to engine component vibrations and loss of engine efficiency. Gas-to-wall heat transfer is strongly promoted under knocking conditions and it is responsible for higher thermal loadings on the solid parts facing the combustion chamber [10]. Moreover, in highly boosted DI engines at low-speed high-load operating regimes, extremely damaging and destructive knocking events called "super-knock" can randomly occur [11], which are explained using a deflagration-to-detonation transition theory [12]. Therefore, knock should be avoided not only to preserve engine durability but also to improve thermal efficiency. The target can be achieved through a reduction of the propagation time needed by the flame, obtained with highly-turbulent flows and/or compact combustion chamber design [13], while increasing the end-gas auto-ignition resistance. The simplest way to improve the auto-ignition delay time is to increase the fuel octane rating using higher RON and higher sensitivity fuels [14]. Sensitivity is defined as S=RON-MON and the effective Octane Index of modern engine/fuel systems is maximized by high-sensitivity fuels [15]. An alternative way to obtain the same effect is the use of additives (e.g. ethers or alcohols) to the original gasoline, as shown by Wei et al. in [16] for pure and gasoline-blended n-butanol and optically analyzed by Merola et al. [17]. The effectiveness in knock suppression of a methanol-water port-injected mixture was numerically confirmed by Berni et al. [18]. The on-the-fly knock mitigation is mainly pursued through Spark Advance (SA) reduction and mixture enrichment. The use of fuel-rich mixtures in GDI engines promotes charge cooling effect and it decreases the temperature of the compressed mixture, increasing the end gas auto-ignition time; however, such strategy favors the emissions of UHC and CO and it reduces fuel economy as shown by Abu-Qudais [19] and by Vafamehr [20]. Fuel enrichment could be avoided through the substitution of the additional fuel with a certain amount of port/direct injected water. In [21] the authors simulated the benefit of port-injected water in a stoichiometric GDI engine and optimized the mass/phasing of the injected water in [22], in agreement with the outcomes on a CFR engine [23]. In [24] similar results were obtained using a larger fraction of injected water (30% of the fuel mass). An expected consequence of water injection adoption is the flame speed reduction caused by its addition to the fuel-air mixture, causing longer flame propagation time. In order to overcome this drawback, the port injection of fuels with high latent heat of vaporization (e.g. alcohols) may be an effective alternative in reducing knock tendency, combining the benefits of increased AI delay times and reduced flame propagation time [25]. The specific fuel consumption is experimentally improved under rich-mixture operation by Liu et al. [26], while the compared benefits and drawbacks of a gasoline-blended water-methanol mixture is simulated in [27]. A different possibility to increase the end-gas AI delay time is represented by the use of cooled EGR. The effect of cooled EGR on KI is about 0.5 RON per % of EGR using commercial gasoline as demonstrated by Alger et al. in [28]. Higher compression ratios can be adopted and therefore engine thermal efficiency improved. Hot internal EGR should be avoided in SI units, as the increased charge temperature negatively affects the knock resistance despite the mentioned charge dilution [29]. Finally, knock resistance can be further improved through higher turbulence levels [30] achieved by using late intake valve closure (LIVC) strategy at high loads or using variable compression ratios [31]. Outcomes of such techniques are compared and validated against 3D CFD simulations in [32]. All the above discussed strategies can be effective in reducing the knock tendency. Such variety of technological scenarios motivates the interest to objectively classify and to model engine KI especially under edge-of-knock operations.

The identification of an acceptable KI is usually carried out through the statistical allowance of a maximum fraction (e.g. 1%) of cycles exceeding a KI higher than a given limit. The use of percentiles is made necessary by the variability of combustion and knock, which can only be characterized through statistics. Even a low probability of highly knocking cycles can seriously damage the engine despite the low average KI. This confirms that the average KI alone is largely insufficient to describe the engine behaviour. Univariate PDFs (Probability Density Functions) and CDFs (Cumulative Density Functions) of KI are widely adopted to characterize the engine knocking tendency and to efficiently synthetize the knock probability, as shown by Spelina et al. [33]. The same authors analyzed more than 700 different operating points (sampling more than 300 cycles for each operation) in [34], confirming that KI can be completely characterized by univariate PDFs of CDFs. Another important finding is in the binomial distribution function motivated by the high number of low-intensity knocking cycles compared to the high-knocking ones. The statistical analysis of the measured data shows that log-normal PDFs best characterize KI distributions on the broad range of operating conditions. This experimental evidence is used in the current study to consistently reconstruct presumed KI distributions using a statistical RANS-PDF knock model developed by the authors in [35]. The same model was validated on a DISI engine in [36] and the presumed log-normal knock statistics were compared to a single-cylinder research engine in [37].

Several studies discussing the CFD modelling of average knock with RANS were presented and validated against experiments by different research groups, using both quasi-dimensional and three-dimensional CFD models. Vancoillie et al. [38] used a fuel-specific Arrhenius formulation for the reaction rate of methanol and ethanol fuels and the average ignition delay was used to integrate a knock precursor species. A similar approach based on the calculation of fuel specific AI delays from chemical kinetics simulations with validated mechanism was developed and used in the past by the authors in a research unit in [39] and correlation with optical knock visualizations was carried out in [40]. However, despite the use of simulated AI delays, the standard RANS approach to knock modelling suffers the inability to reproduce the inherently stochastic nature of knock. This is an intrinsic yet severe limitation for this type of models. The dramatic impact of Cycle-to-Cycle Variability (CCV) on all the in-cylinder physical processes (e.g. fuel-air mixing, turbulent combustion, etc.) motivates the adoption of a Large-Eddy Simulation (LES) approach, where the largest flow structures are resolved allowing the simulation of flow unsteadiness. A rigorous analysis of CCV can only be carried out through LES, as engine knock of each cycle depends on all the CCV-affected preceding processes. Despite the still demanding cost of LES analyses in ICEs, several studies of this kind were presented by the authors in [41] using a tabulated knock model described in [42] and by Robert et al. [43]. Similar studies numerically described the cycle-resolved knock onset in a small-displacement SI engine [44] and discussed the effect of the wall thermal field con knock CCV in [45]. They showed that the simulated combustion CCV was able to replicate the degree of instability measured at the test-bench for a premixed isooctane-air engine at several SA. These examples demonstrated the investigation insight made possible by LES and the possibility to explain individual misfiring cycles or cycle-specific knocking events, thus allowing a direct comparison between simulation results and engine test-bench output. However, the cycle-resolved description of knock provided by LES is often far from the experimental practice where, usually, knock is only characterized by its statistics. This discrepancy, together with the severe computational cost, prevents the application of LES in the design process of production engines.

In the above context the definition of a new approach for knock modelling emerges as a necessary bridge between the poorly representative RANS "ensemble average knock" and the expensive CPU effort of a multiple cycle LES study. The approach is based on the RANS formalism for averaged quantities, combined with the use of transport equations for variances of physical conditions allowing to estimate a knock probability or a fraction of knocking cycles. Pursuing the same concept developed by Linse et al. [46] and relying on transport equations for mixture fraction and enthalpy variances, a statistical RANS model described in [35] was proposed to infer not only the average KI but also the presumed distribution of knock intensity, and the model validation was carried out on both an optically accessible research engine and a production unit. Conversely from the use of a traditional RANS approach, the use of the developed statistics-based knock model gives a quantitative information regarding the presumed fraction of knocking cycles affecting the mean simulation for a given operating condition, thus enhancing the consistency of a RANS simulation of knock with a typical test-bench acquisition dataset.

The present study aims at comparing the CFD outcomes in terms of knock prediction using the most suitable CPU expensive multi-cycle LES and the widely adopted CPU efficient RANS methods. In particular, 25 consecutive cycles of a currently produced GDI engine operated at full load and 7000 rpm engine speed are simulated using LES over a wide range of SAs. For each spark time, LES is coupled with a validated knock model [39] based on chemistry-derived auto-ignition delays representative of a European RON-98 gasoline. The CFD results are compared to the cycle-resolved measured KI at Knock Limited Spark Advance (KLSA), proving the suitability of this kind of approach in predicting both combustion and knock variability (i.e. knock statistics). The CFD analysis is repeated in a RANS framework using the identical chemistry-based library and a statistical knock model. The aim is to compare statistical information inferred through RANS and the ones derived by multi-cycle LES for SA variations. Both CFD methods show promising results in predicting knock probability. Whereas in LES statistics are derived from cycle-resolved flow solutions, thus providing indications of the root causes behind highly knocking cycles, statistical RANS allows to predict with a reasonable accuracy the fraction of knocking cycles with dramatically shorter CPU times.

The relevance of this study lays in the proven similarity of the knock statistics obtained using the developed RANS-PDF knock model with respect to multi-cycle LES and experiments for several SA. The predicted fraction of knocking cycles is in very good agreement between experiments, LES and RANS-PDF, while a standard RANS model relevantly underestimates KI and it gives no information on knock statistics. Such evidence substantially expands the field of applicability of RANS-based models for knock prediction in industrial applications, e.g. development of ICEs.

2. Materials and Methods

2.1 Investigated Engine and Experimental Measurements

A direct-injected V-shaped 8 cylinder turbocharged SI engine is modelled. The main geometrical characteristics are typical of modern high performance GDI units in terms of B/S ratio (slightly higher than one) and volumetric compression ratio (approx. equal to 10). In Figure 1 the fluid domain considered in the CFD analyses (the same for RANS and LES) is highlighted in red, i.e. cylinder number 1 including the in-head portion of the intake ports and the exhaust port up to the turbine junction.
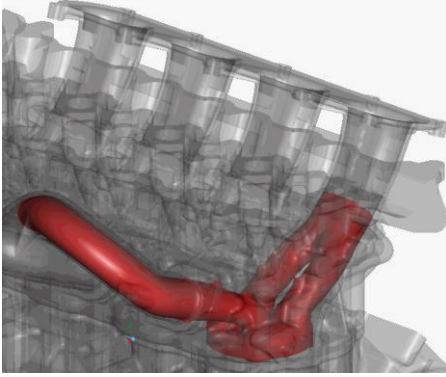

Figure 1: Investigated engine geometry; in red the fluid domain considered for CFD simulations.

The analysed operating condition is the full-load peak power one at the operating speed of 7000 rpm, with a boost pressure of 0.5 bar and using a RON-98 commercial gasoline. In order to avoid knock onset and limit the turbine inlet temperature, the fuel/air mixture is enriched (nominal lambda index of 0.8). The main engine parameters are reported in Table 1. In-cylinder pressure measurements are performed with a piezo-electric sensor featuring a $\pm1\%$ accuracy and 240 consecutive engine cycles are recorded for each cylinder with a crank angle resolution of 0.5 CAD. In Figure 2 the in-cylinder pressure traces for the recorded cycles are reported. The average pressure peak is 87 bar and the maximum/minimum ones are 105.5 bar and 65.2 bar respectively. A standard deviation of 7.1, leading to a peak pressure coefficient of variation (CoV) of 8.15%, is measured.

Table 1: Main geometrical and operation parameters for the investigated engine.

Bore / Stroke [mm]	86.5 / 80.8
Geometrical Compression Ratio	10
Conn. Rod Length [mm]	141.25
Operating Speed [rpm]	7000
Valves per cylinder	4
Fuel	Gasoline (RON-98 E0)
Nominal Lambda Index	0.8 (stratified charge)
Knock-Limited Spark Timing [CAD bTDC]	12
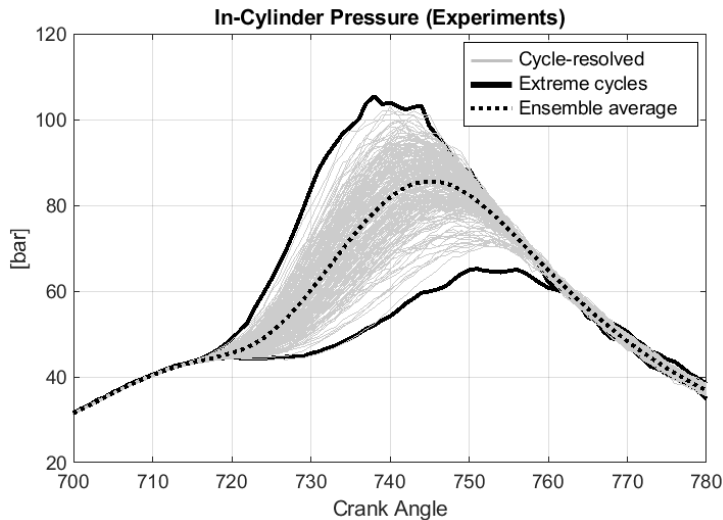
Figure 2: In-cylinder pressure traces of 240 consecutive cycles (grey); the highest and the lowest peak pressure cycles are in solid black lines, ensemble average is in dashed black line.

The pressure signal is filtered with a pass band filter (8-25 kHz), to eliminate both the low-frequency noise of regular combustion and the high-frequency data whose signal-to-noise ratio is affected by the sensor natural frequency oscillations. In-cylinder pressure is measured using a flush-mounted Kistler 6061B pressure transducer, side-positioned in the combustion chamber. The cycle-resolved $MAPO_i$ (Maximum Amplitude of Pressure Oscillations) is assumed as KI indicator and it is calculated as in Eq. 1, where $|\tilde{p}_i|$ is the filtered pressure of the *i-th* cycle and the integration window is defined from ϑ_1=-40 CA aTDC to ϑ_2=90 CA aTDC.

$$MAPO_i = max\left(|\tilde{p}_i|_{\vartheta_1}^{\vartheta_2}\right)$$
Eq. 1

For the analyzed condition the engine is operated at a KLSA equal to 12 CAD bTDC. In the experimental practice the cylinder-specific KLSA is defined as the most advanced spark timing guaranteeing 99% of the cycles with a maximum MAPO lower than the assigned limit. This is calculated as MAPO$_{max}$=rpm/1000 [bar], i.e. MAPO$_{max}$=7 bar in this study. A safety margin is retained by further reducing the SA by 0.5 CAD. This means that at the adopted SA none of the 240 cycles exceeds the MAPO$_{max}$ threshold, while increasing the SA by 0.5 CAD more than 1 cycle will exceed the threshold. The cycle-resolved MAPO as a function of the pressure peak at KLSA is reported in Figure 3: as expected none of the 240 considered cycles goes over the MAPO$_{max}$=7 bar knock threshold. The maximum and the average measured KI in the analyzed condition are 5.9 and 1.7 bar, respectively. It is important to notice that the minimum KI is always non-zero even in knock-free cycles, as a consequence of a background noise (e.g. pressure oscillations induced by regular combustion) measured by the transducer and not related to engine knock.
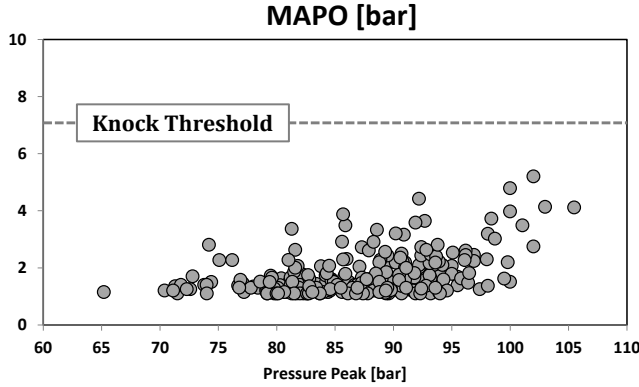

Figure 3: Measured cycle-resolved MAPO for the 240 consecutive engine cycles dataset as a function of the pressure peak.

2.2 CFD Methodology

The numerical grid covers the combustion chamber and the intake and exhaust ports for both RANS/LES simulations. The mesh resolution is increased near the spark plug electrodes, which are meshed in the geometry in order to account for the electrodes-flame aerodynamic interaction during the first stage of combustion. The resulting number of in-cylinder cells is about 1M/1.8M at TDC/BDC, resulting in an average cell size of 0.5mm. Previous studies on the same engine in LES framework demonstrated that the adopted grid is suitable for LES at the chosen operating condition, as demonstrated by length-scale and energy resolution in [47] and by Proper Orthogonal Decomposition in [48]. Time-varying pressure and temperature boundary conditions (BCs), derived from a tuned 1D model of the engine, are applied at both the intake and exhaust ports; the same cyclic BCs are applied for RANS and LES cases for all the simulated cycles. This approach is suitable for multi-cycle in-cylinder analyses considering the negligible effect of pressure and temperature variability at the intake and exhaust sections on combustion CCV, which is dominated by turbulence generated during valve flow [49]. Identical fixed and uniform wall temperatures are applied in RANS and LES models, and to consider in a simplified way the temperature variation on different engine components the domain is divided as illustrated in Table 2. Wall heat transfer is simulated using the recently developed GruMo-UniMORE model [50], whose improved results compared to common wall heat transfer models are discussed in [51].

Table 2: Wall temperatures adopted in the CFD analyses (both RANS and LES simulations).

CFD Wall Temperatures

Piston Crown	540 K	Exhaust Valve Stem	900 K
Cylinder Liner	450 K	Exhaust Valve Face	950 K
Cylinder Head	470 K	Exhaust Port	450 K
Intake Valve Stem	500 K	Centre Spark Electrode	973 K
Intake Valve Face	640 K	J Spark Electrode	1173 K
Intake Port	400 K		

Turbulence is modelled in the RANS framework using the k-ε RNG model for compressible flows, whereas LES analyses adopt the static Smagorinsky [52] model for sub-grid scale viscosity, where a c_s=0.202 constant is used. In order to achieve cyclic convergence of RANS results (i.e. to neglect initialization-related effects, such as the fuel backflow in the intake line in the first simulated cycle), three consecutive engine cycles are simulated. The effect of the imposed IC on the first LES cycle is minimized imposing as resolved flow field the mean one deriving from the third RANS cycle; in addition to this, the first 2 cycles of the simulated 25 are not considered in the statistical analysis. For the high-pressure fuel injection simulation, a pre-atomized population of Lagrangian particles is assigned to each of the 7 injector nozzles in both RANS and LES framework [53]. The secondary break-up is modelled by means of the Reitz model [54]. Also the fuel representation is common to RANS and LES, with a single component fuel able to match the global distillation curve of the real gasoline used in the experiments.

Combustion is modelled using the ECFM-3Z version for the simulation of flame propagation in RANS [55] and the ECFM-LES in LES [56], sharing a laminar flame speed (LFS) definition through a chemistry-based polynomial fitting for full-load engine-like conditions [57]. The methodology was applied to gasoline and n-butanol combustion in a single-cylinder research engine in [58] and extended to the low-pressure range typical of part-load conditions in [59]. The ignition treatment differs between RANS and LES: in RANS a relatively simple algebraic model based on a Flame Surface Density (FSD) for RANS (FSD-RANS) deposition after a kernel growth delay (internally calculated) is used and purposely calibrated to match the experimental early burn rate [60]. In LES, considering the first-order relevance of the ignition process and early flame development on combustion CCV and knock, an advanced ignition model (ISSIM-LES, Imposed Stretch Spark Ignition Model) developed by Colin et al. [61] is used for the current analyses. In ISSIM-LES the FSD-LES transport equation is modified during the ignition stage with the addition of terms explicitly devoted to the sub-grid scale treatment of FSD. This is needed in order to accurately simulate flame size as small as the typical cell size. The adopted model constitutes a remarkable simulation improvement over traditional SI models based on the deposition of a resolved profile of fully-burnt gases [62] and it was demonstrated to explain the governing reasons for CCV origin in different SI engines in [63].

2.3 Knock Modelling

Auto-ignition delay times are calculated off-line using detailed chemistry in constant pressure reactors for a wide set of pressure, temperature, equivalence ratio and EGR conditions. The DARS chemistry solver, licensed by Siemens PLM, is used. Thermo-physical states are intended to cover all the possible conditions experienced by the end-gases during the compression/combustion stages. Calculated ignition delays are stored in an indexed database (Look-Up Table, LUT). The AI delay library is then used at each time-step and fluid cell to interpolate an ignition delay time for the CFD solver [42]. The same anti-knock quality of the RON-98 European gasoline is reproduced using the semi-detailed TRF mechanism from Andrae et al. [64], composed by 143 chemical species; it is used to create a fuel surrogate model consisting of a ternary blend of Toluene/Isooctane/n-Heptane (37.6%/8.2% /54.2% by mass fraction, respectively). This is defined following the mapping method from RON/MON space to TRF composition proposed by Morgan et al. [65]. Time integration of the instantaneous and local reactivity is carried out in both RANS and LES framework using the two-species Lafossas integral knock model [66] as in Eq. 2, in which the two species $\tilde{Y}_{IG}$ and $\tilde{Y}_{TF}$ are the cumulative knock precursor and the fuel tracer, respectively. When the condition $\tilde{Y}_{IG} = \tilde{Y}_{TF}$ is locally verified, knock is triggered at the same AI delay τ_d predicted by detailed chemistry. Despite the same formalism for knock prediction (i.e. the same LUT of AI delay times) is adopted to simulate the engine knock tendency both in LES and RANS, LES can account for the cycle-resolved knock, as a consequence of the simulated CCV of mixture formation (Φ and EGR dilution), pressure and temperature evolution.

$$\frac{d\tilde{Y}_{IG}}{dt} = \tilde{Y}_{TF} \cdot \frac{\sqrt{\tau_d^2 + 4(1-\tau_d)\,\tilde{Y}_{IG}/\tilde{Y}_{TF}}}{\tau_d} \qquad \text{Eq. 2}$$

In RANS analyses a statistical version (RANS-PDF) of the knock model is used, which is developed to infer knock statistics from RANS equations and whose details can be found in [35]. The model details are briefly recalled here for the sake of completeness. Two additional equations for the variances of mixture fraction Z and conditional unburnt enthalpy h_u ($\widetilde{Z''^2}$ and $\widetilde{h_u''^2}$, respectively) are solved in Eq. 3 and 4, accounting for ensemble-averaged variance generation/dissipation based on local gradients and turbulence intensity. They are derived from the general formulation of the variance transport equation in RANS framework. The turbulent relaxation time-scale $\tau_Z(Re_t)$ is dynamically calculated using the approach proposed by Fox [67]. The unburnt temperature $\tilde{T}_u$ and its variance $\tilde{T}_u''$ are calculated from $\tilde{h}_u$ and $\tilde{h}_u''$ through the mixture specific heat.

$$\frac{\partial \bar{\rho}\widetilde{h_u''^2}}{\partial t} + \frac{\partial}{\partial x_j}\left[\bar{\rho}\tilde{v}_j\widetilde{h_u''^2} - \left(\bar{\rho}D_{\widetilde{h_u''^2}} + \frac{\mu_t}{\sigma_t}\right)\frac{\partial \widetilde{h_u''^2}}{\partial x_j}\right] = 2\frac{\mu_t}{\sigma_t}\left(\frac{\partial \widetilde{h_u}}{\partial x_j}\right)^2 - \frac{\bar{\rho}}{\tau_Z(Re_t)}\widetilde{h_u''^2} \qquad \text{Eq. 3}$$

$$\frac{\partial \bar{\rho}\widetilde{Z''^2}}{\partial t} + \frac{\partial}{\partial x_j}\left[\bar{\rho}\tilde{v}_j\widetilde{Z''^2} - \left(\bar{\rho}D_{\widetilde{Z''^2}} + \frac{\mu_t}{\sigma_t}\right)\frac{\partial \widetilde{Z''^2}}{\partial x_j}\right] = 2\frac{\mu_t}{\sigma_t}\left(\frac{\partial \tilde{Z}}{\partial x_j}\right)^2 - \frac{\bar{\rho}}{\tau_Z(Re_t)}\widetilde{Z''^2} \qquad \text{Eq. 4}$$

Therefore, local Z and T_u are described not only by a unique value ($\tilde{Z}$ or $\tilde{T}_u$, as in the case of standard RANS) but also by variances $\tilde{Z}''$ and $\tilde{T}_u''$, thus depicting a statistical thermal-mixing field. The joint variation of Z and T_u is represented by a simplified Gaussian bivariate distribution model (Figure 4) in which the effect of local turbulence on temperature and mixture fraction distribution is shown. Among other possibilities (e.g. Weibull or Beta-distributions, etc.), the bivariate Gaussian model is chosen to keep the model as simple as possible.
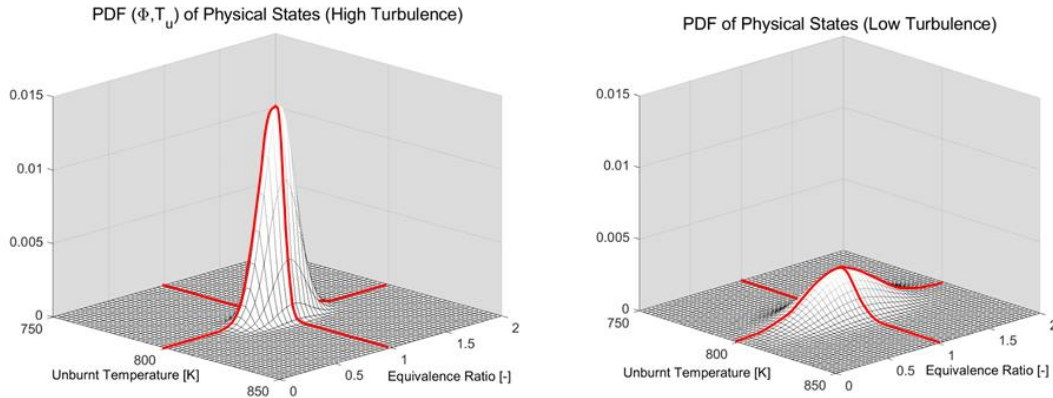
Figure 4: Bivariate PDF of the in-cell physical states for the same mean condition (red line): decreasing turbulence intensity levels (from left to right) lead to more probable far-from-average states.

The continuous PDF of the in-cell states is discretized into 9 steps for both Z and T_u (i.e. 81 possible (Z,T_u) states) covering 2 standard deviations (i.e. 95% probability) for each fluid cell. An AI delay for each (Z,T_u) combination is interpolated from the LUT, thus describing a distribution of in-cell reactivity; a 2-moments framework is then introduced to synthetize the calculated field and to account for both the average in-cell average reactivity and its faster-than–average deviation (e.g. earlier-than-average AI):

- A cell-averaged ignition delay time ($\tilde{\tau}_d$) is calculated from all the (Z,T_u) states using the bivariate PDF as a weight. In this way higher probability states (e.g. the $(\tilde{Z},\tilde{T}_u)$ condition) are considered as more representative in the averaging process than lower-probability ones, as schematized in Figure 5.
- As the $\tilde{\tau}_d$ value alone would not be sufficient to fully represent the reactivity distribution, a second moment is added, i.e. the calculated standard deviation τ_{RMS}.

The model transports a presumed distribution of reaction rates, hence earlier-than-average knock can be predicted based on the assumed distribution function: while the use of the PDF-weighted average $\tilde{\tau}_d$ leads to the mean knock prediction, its substitution with delay times reduced by 2 or 3 standard deviations (τ_d'' and τ_d''', respectively, as reported in Table 3 and schematized in Figure 6) is in charge of estimating knock-proner situations. Clearly, the probability of the knocking event associated with τ_d'' or τ_d''' delay times lowers as they correspond to far-from-average ($\tilde{Z},\tilde{T}_u$) conditions. Following the transport of infinite knocking realizations operated by the statistical RANS knock model, the heat release by AI is numerically de-activated (passive model) in order preserve an AI prediction not influenced by earlier AI realizations.
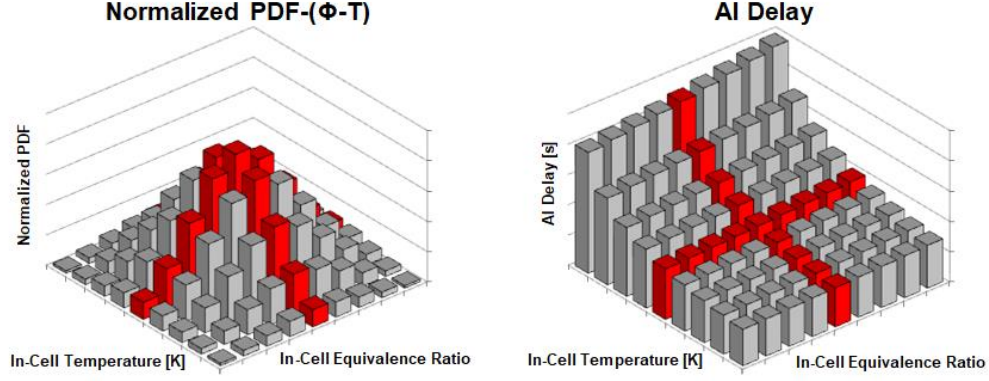
Figure 5: Discretized bivariate PDF (left) and AI delay time from look-up table for each represented physical status. The mean condition is highlighted in red.

Table 3. Knock realizations and AI delays.

Meaning	Name	AI Delay
Average Knock	$\tilde{\tau}_d$	$\tau_{PDF_{aver}}$
Faster-than-average knock (by 2 RMS)	τ_d''	$\tau_{PDF_{aver}} - 2 \cdot \tau_{RMS}$
Faster-than-average knock (by 3 RMS)	τ_d'''	$\tau_{PDF_{aver}} - 3 \cdot \tau_{RMS}$
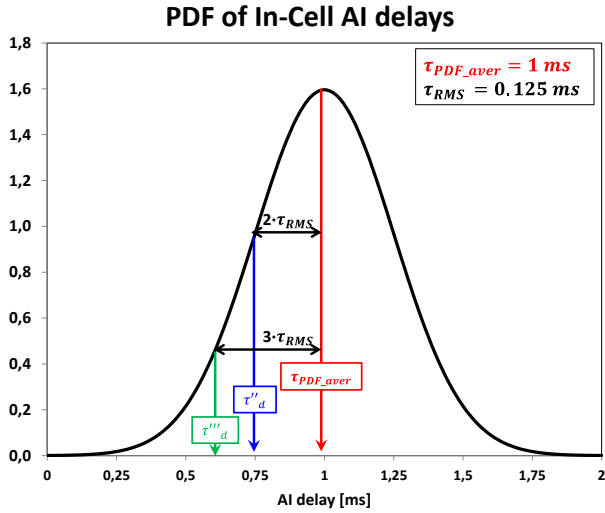
Figure 6: Gaussian PDF of auto-ignition delay times obtained for each computational cell.

However, for the sake of understanding, a visual representation of the heat released by the several AI events is shown by arbitrarily choosing one of the AI delays transported by the PDF function and enabling the specific auto-ignition event (active version of the model). In this way, knocking events with high/low KI and probability can be simulated together with the associated heat release. In particular, given the interest towards earlier-than-average knocking events, an AI delay decrease is of high interest: while the knock probability decreases, the related KI increases. When the AI heat release is activated, the KI associated to the knocking event is calculated and it is used to directly compare CFD and experiments. To this aim, the most reasonable choice would be to use the same knock index, e.g. MAPO. The numerical simulation of the pressure wave propagation could be used to directly estimate MAPO from CFD; however, this would result in a very challenging task: time-steps and grid density should be well resolved to adequately comply with the CFL condition. Also, the pressure signal should be monitored at the very same position as the pressure transducer and the CFD signal should be filtered with the same frequency as the raw transducer trace. In order to avoid these issues and to retain a reasonable CPU efficiency, an alternative

method to estimate the pressure rise given by knock is proposed. It is based on the energy released by AI and it can be used in both RANS and LES frameworks. The Estimated MAPO function (eMAPO, Eq. 5) is defined as the pressure rise corresponding to the constant volume (instantaneous) combustion of the auto-ignited fuel. In Eq. 5 p_{KO} is the in-cylinder pressure at KO, $m_{f,knock}/m_{f\,cyl}$ is the fraction of the AI fuel over the gas mixture, K_i is the fuel lower heating value, T_{KO} is the unburned temperature at KO, while c_p and MW are the specific heat and the molecular weight of the unburned mixture and R_u the universal molar gas constant.

$$eMAPO = p_{KO}\frac{m_f\,knock}{m_f\,cyl}\frac{K_i}{T_{KO}\left(c_p - \frac{R_u}{MW}\right)}$$

Eq. 5

The eMAPO index derives from the Knock Severity Index (KSI) proposed by Klimstra in [68] relating the knock pressure wave to an isochoric auto-ignition, and it shares the same goal to be an objective and easily measurable indicator for KI. Moreover, it can be directly compared to the experimental MAPO. In fact, all the variables in Eq. 5 are available from CFD simulations (irrespectively RANS and LES), while the fraction of knocking fuel is derived from the heat released by AI. This energy-based approach permits to estimate the knock pressure rise in RANS and LES frameworks through the eMAPO and using the same limit as in the experiments (eMAPO$_{max}$=7 bar).

The cycle-resolved eMAPO is calculated in LES simulations and the distribution from the 23 consecutive cycles for each simulated SA is used to reconstruct a log-normal distribution of KI. Then, the associated CDF is used to estimate the knock probability below/above the eMAPO$_{max}$ limit.

In statistical RANS, the average KI is estimated using eMAPO$_{AVER}$ by activating the AI heat release associated with the average knock precursor (corresponding to $\tilde{\tau}_d$), while the eMAPO$_{RMS}$ is inferred as the difference between the eMAPO^n associated to the faster-than-average knocking event and eMAPO$_{AVER}$. This is formalized in Eq. 6, in which eMAPO^n is the one resulting considering as source term for the knock precursor τ_d^n divided by n.

$$eMAPO^n{}_{RMS} = (eMAPO^n - eMAPO_{AVER})/n$$

Eq. 6

3. LES Results

As stated earlier, in order to get rid of the initial conditions, the LES analyses start from the third (cyclic converged) RANS cycle, following which 2 LES cycles are used and discarded to allow a smooth transition from RANS to LES. Then, results are analyzed for the remaining 23 LES cycles. In-cylinder pressure traces of these 23 cycles are reported in Figure 7 (red lines) and compared to the experimental bandwidth. For the sake of graphical clarity, only the highest, lowest (black solid lines) and ensemble average (black dashed line) pressure traces are reported.
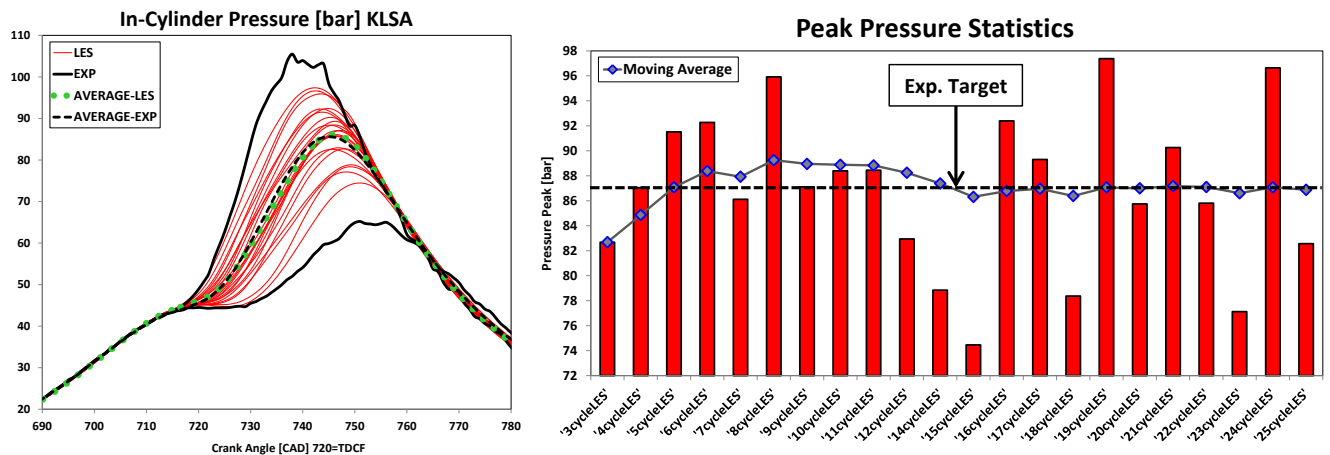

Figure 7: In-cylinder pressure traces of the 23 considered LES cycles (left) and pressure peak statistics (right) comparison with the experiments

All the simulated cycles are within the experimental envelop and the agreement is excellent also comparing the ensemble average experimental and simulated pressure curves. The 23 realizations from CFD are not able to cover the entire

experimental CCV, and this can be ascribed to the simulation of CCV-promoting factors only related to turbulence, while factors such as spray shot-to-shot variability or spark energy cyclic fluctuations are neglected. As a result, a slight underestimation of combustion CCV is obtained: the simulated RMS of pressure peak is 6.3 bar (instead of 7.1), while the pressure peak Coefficient of Variation (CoV) is 7.2% (instead of 8.15%).

Despite the number of simulated cycles is much lower than the number of experimental counterparts, converged values for pressure statistics are met. The convergence of average pressure peak is met after about 15 simulated cycles: considering the last 10 cycles (from cycle 15 to cycle 25), the average pressure peak variation is lower than 0.8 bar, while considering the last 5 cycles the maximum variation is lower than 0.5 bar. The same consideration is done in terms of pressure peak RMS and CoV, reported in Figure 8. Despite the general increasing trend moving from cycle 15 to cycle 25, the pressure peak RMS increase is lower than 0.4 bar while the CoV increases by 0.38%. This confirms that the CCV underestimation is more related to modelling assumptions than to the number of simulated cycles. For this reason, the LES dataset does not include additional simulated cycles.
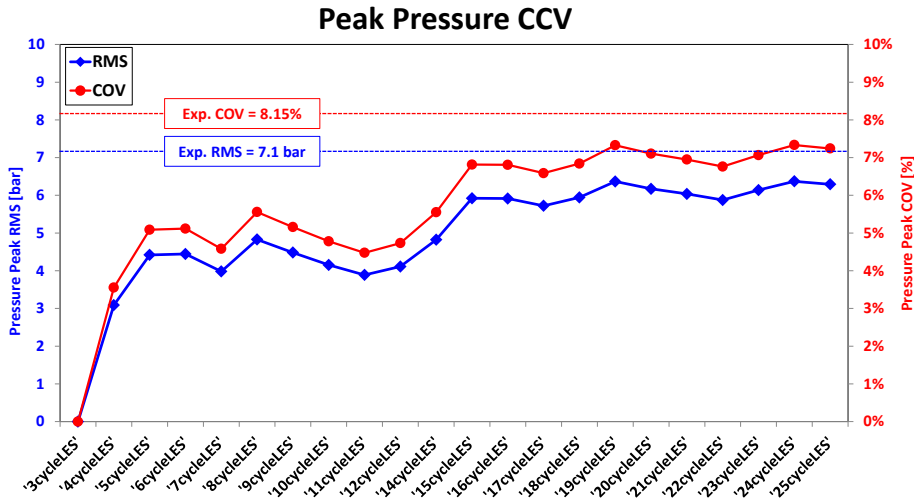

Figure 8: Pressure peak standard deviation (RMS, blue) and Coefficient of Variation (COV, red) increasing the number of LES simulated cycles.

The HRR of all the simulated cycles is monitored in its separated contributions: the portion released by premixed combustion and the one released by AI, as calculated by the combustion model. Both the global HRR (left) and the portion released by AI (HRR_{AI}, right) are illustrated in Figure 9, together with the ensemble averaged HRR: the effect of AI on the average pressure trace is negligible. This is also confirmed by the average HRR_{AI}, which is more than one order of magnitude lower than that released by premixed combustion. However, despite the absence of sensible knock in the average pressure and HRR signals, few isolated cycles experience a non-negligible KI.
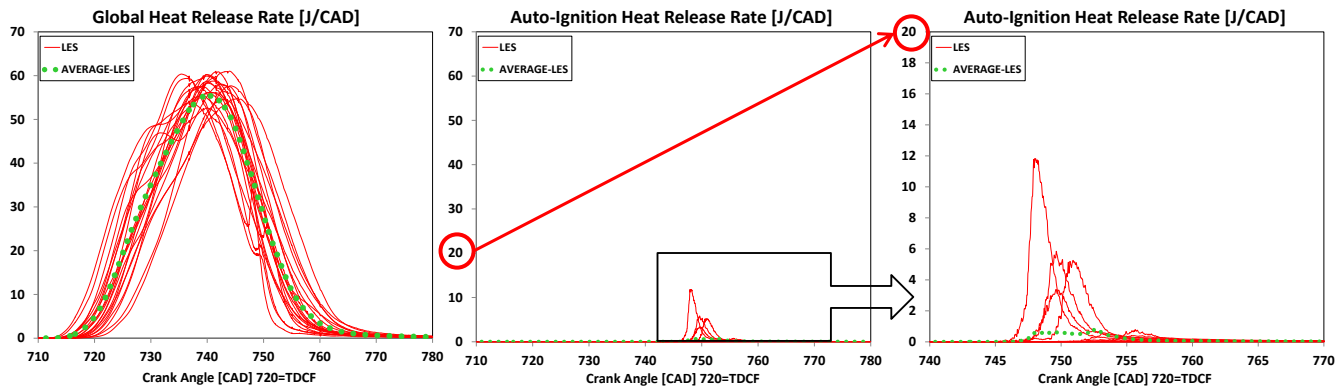

Figure 9: Global rate of heat release (left) and Auto-ignition heat release rate (center and right) of the 23 simulated LES cycles.

The fraction of heat released by AI (H_{AI}) is calculated through an integration in time of the HRR_{AI} curve of each cycle (in Figure 10), which is finally normalized on the overall heat. Similarly to the pressure peak (Figure 8), also the average H_{AI} converges to a stable value of 0.29% after 15 cycles. In the simulated KLSA condition the average amount of HRR_{AI} is three

orders of magnitude lower than the total one (i.e. approximately 8J over 2600J), and 16 cycles over 23 show a H_{AI} fraction lower than the average H_{AI}. In particular, more than half of the simulated cycles (12 cycles) show an almost null HRR_{AI}, with a fraction of $H_{AI}<0.02\%$, while the H_{AI} of 3 cycles overcomes by one order of magnitude the average H_{AI}. These results confirm the limitations and poor meaning of the average KI, given the stochastic nature of knock. Such limitation is even more critic at edge-of-knock conditions such as the KLSA one here analyzed, in which the KI measured for the upper outliers largely overcomes the KI of the majority of knock-free cycles.
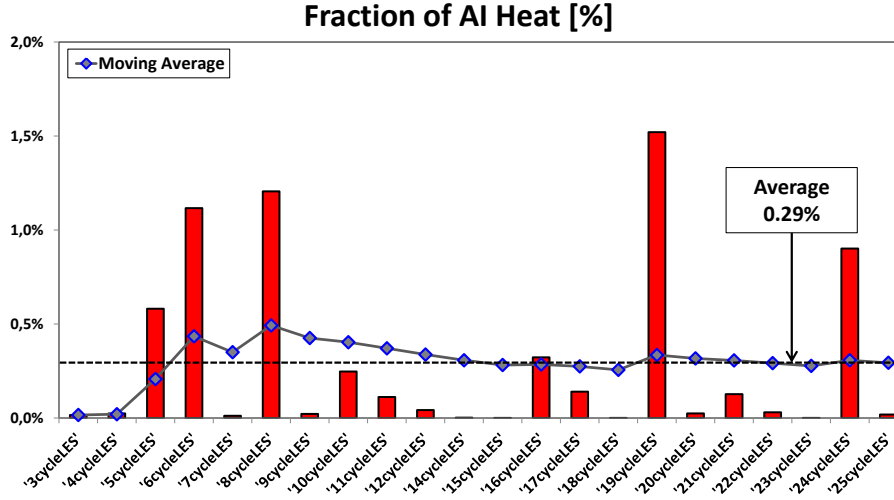

Figure 10: Fraction of heat released by auto-ignition in the 23 analyzed LES cycles.

The cycle-resolved eMAPO (Eq. 5) is calculated dividing the HRR_{AI} by the fuel lower heating value and by the amount of auto-ignited fuel. This is used to compare the KI of CFD results with the experimental outcomes. Attention is paid to the background noise affecting the experimental signal, which must not be confused with knock-related trace: the pressure rise given by the instantaneous combustion of the AI fuel is null when no heat is released by AI. As a consequence, in most of the simulated cycles the eMAPO value is almost zero, while the experimental MAPO value is always higher than MAPO =1.1 bar, motivated by the presence of a regular combustion noise (not related to knock). In order to fairly compare CFD and experiments, the same level of background noise (1.1 bar) is superimposed to the calculated eMAPO value. Finally, the comparison between KI from experiments and CFD is reported in Figure 11 as a function of the pressure peak.
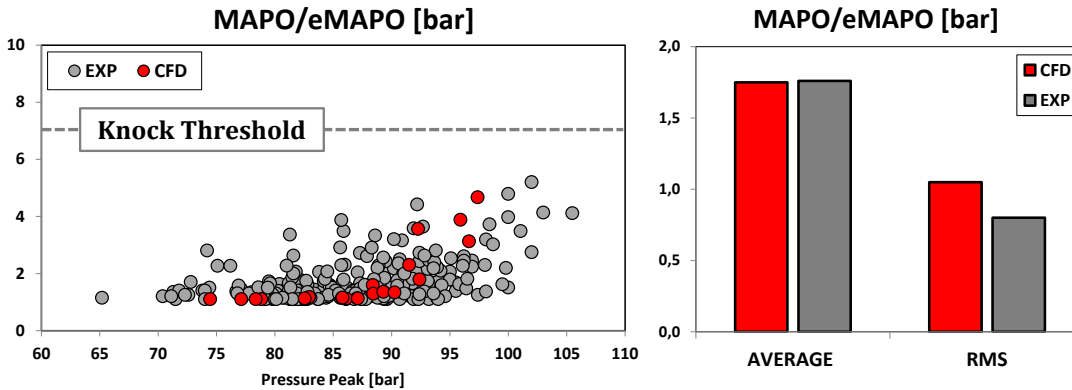

Figure 11: Comparison between LES and experimental KI (eMAPO and MAPO, respectively) at KLSA.

The average KI of the 23 analyzed cycles is in good agreement with the experimental measurements, while the maximum KI and pressure peak are underestimated. However, the rate of increase of KI with the pressure peak is quite well reproduced by the CFD model. The analysis of the eMAPO shows that none of the simulated cycles overcomes the $eMAPO_{max}=7$ bar knock limit. This confirms the knock-safe operation indicated by the experiments. The simulated average KI is almost the same as the experimental one, whereas the CCV of KI, here quantified through the eMAPO standard deviation ($eMAPO_{RMS}$), is slightly overestimated in CFD (1.05 instead of 0.8). The overestimation of the KI variability may be reduced by simulating more cycles, as shown by the decreasing trend in the evolution of the $eMAPO_{RMS}$ (Figure 12). After an initial $eMAPO_{RMS}$ increase

when the first knocking events are detected (cycle 3 to cycle 8), a later $eMAPO_{RMS}$ decrease and convergence towards the experimental value (from cycles 8 to 18) is observed. The detection of an outlier cycle in terms of KI (similar to the maximum experimental one) as the 19th cycle leads to a new jump in the $eMAPO_{RMS}$.
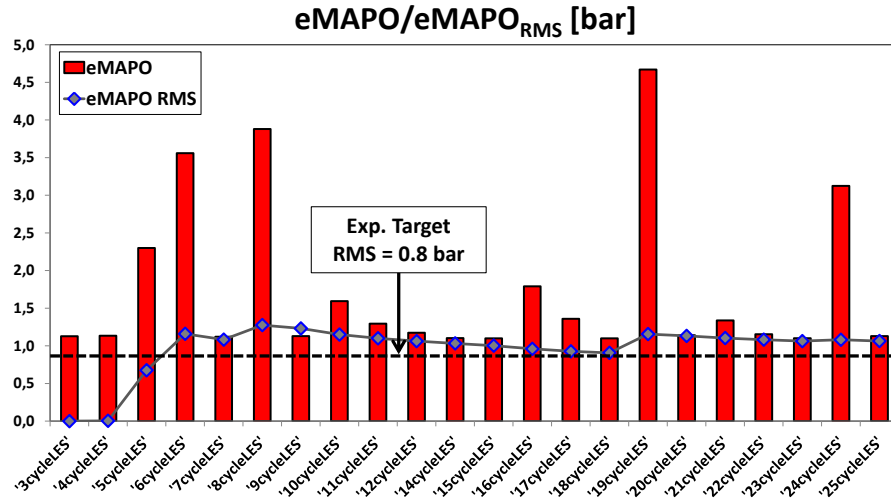

Figure 12: Knock intensity (eMAPO) of the 23 considered LES cycles and cycle to cycle evolution of the eMAPO standard deviation

Once the model reliability is assessed both in terms of combustion development and KI prediction, multi-cycle LES is used to predict the engine behavior under operations in which no experimental data are available. In particular, the SA is increased with a step of 0.5 CAD (as in the experimental practice for the KLSA evaluation) reaching a maximum SA increase of 2 CAD (KLSA+2.0). The in-cylinder pressure traces from the CFD spark-sweep simulations are reported in Appendix 1, while in Figure 13 (left) the cycle-resolved eMAPO as a function of the pressure peak is reported.
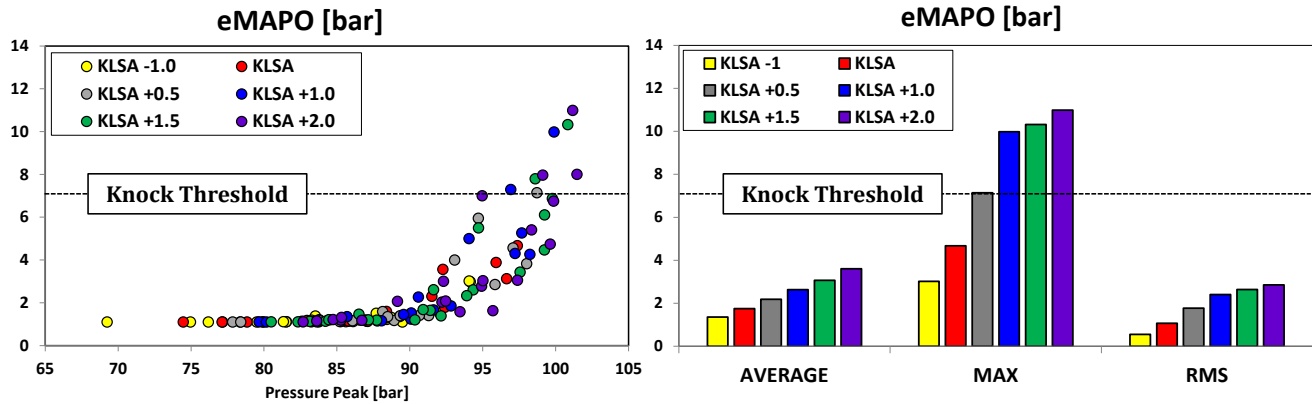

Figure 13: LES Cycle-resolved knock intensity (eMAPO) as a function of the pressure peak changing the spark time (left), average/maximum and standard deviation of LES knock intensity (right) changing the spark time.

As expected, both pressure peak and KI increase for advanced combustions. Considering the average KI alone (i.e. $eMAPO_{AVER}$), despite the wide SA sweep operated in CFD moving from KLSA-1.0 to KLSA+2.0, an increase lower than 2 bar is observed. This is still well below the $eMAPO_{max}=7$ bar knock limit even under KLSA+2.0 operation.

A more complete framework comes from the $eMAPO_{RMS}$ increase with SA, which combined with the $eMAPO_{AVER}$ trend draws a statistic picture where an increasing population of cycles exceeds the $eMAPO_{max}$. As the $eMAPO_{RMS}$ magnitude is comparable to $eMAPO_{AVER}$, it is clear how incomplete a knock characterization can be if based only on average KI without any information regarding its variability. A further confirmation of the robustness of the presented methodology comes from the simulated SA sweep, where an increase of 0.5 CAD from KLSA leads to 1 out of 23 cycles overcoming the $eMAPO_{max}$ threshold (this corresponds to 4.3% of the sample, given the reduced statistical population). This means that CFD can correctly predict the experimental KLSA considering the same statistical knock analysis as the test bench, i.e. the SA for which more than 1% of cycles exceeds a given KI threshold. In this case, moving from KLSA to KLSA+0.5 and KLSA+1.0 the fraction of knocking cycles is 0%, 4.3% and 8.7%, respectively: 0,1 and 2 cycles overcome the threshold. In other words, it would not

be possible to establish the SA for which 1% of cycles is knocking unless at least 100 realizations are available. Whereas this is common for experiments, it still represents a gigantic task for LES analysis of ICE.

In order to overcome this limitation, the knock results from the reasonable number of LES cycles are used to define a fitted log-normal distribution function for eMAPO. The results of this analysis are reported in Figure 14, in which the log-normal PDF fit of experimental and CFD datasets are reported for all the considered SA. A similar KI distribution is found comparing CFD and experiments for KLSA operation, while broader and more skewed distributions are obtained increasing SA.
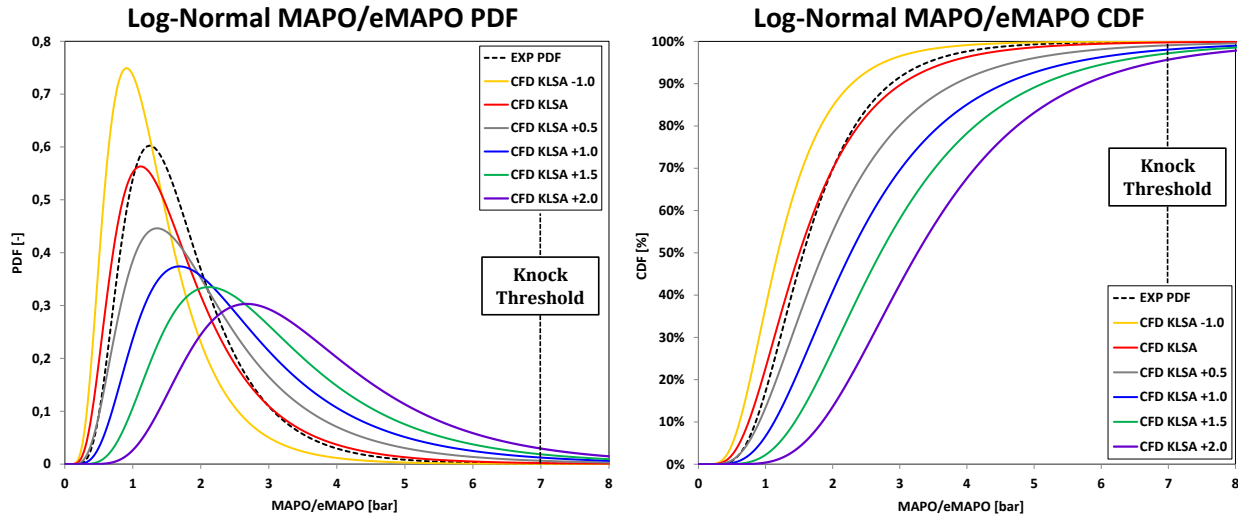

Figure 14: Log-normal PDF (left) and CDF (right) of KI changing the spark time from the LES average eMAPO and eMAPO$_{RMS}$; in black dotted line the log-normal fit of the experimental dataset at KLSA is reported.

The rightmost portion of the log-normal fit overcoming the MAPO$_{max}$=7 bar in the CDF quantifies the fraction of knocking cycles. The predicted value is reported in Figure 15 for all the SA, showing that the prediction of the KLSA using LES and log-normal fitting functions for KI is fully consistent (0.5 CAD higher) with the experimental one. For this SA the experiments show a percentage of knocking cycles equal to 0.93%, which almost doubles for a further +0.5 increase in SA.
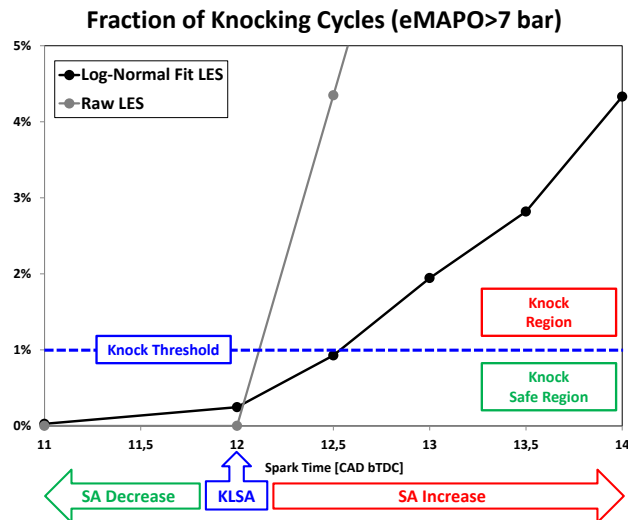

Figure 15: Estimated fraction of knocking cycles from LES results; raw LES dataset (grey line) and log-normal shaped fit (black line) for several SAs.

4. RANS results

The simulation of the same engine operation and SA sweep is then performed using the RANS framework; simulations share as many sub-models as possible with the LES counterpart, as described in the Numerical Models section. This choice is

deliberately made to coherently compare results obtained through different numerical approaches. The adopted combustion and ignition models are accurately tuned to reproduce the average in-cylinder pressure trace at KLSA. In Figure 16 (left) the comparison of average in-cylinder pressure from RANS (blue line) and LES (red line) is reported, together with the ensemble average experimental cycle and the upper/lower limits of the experimental envelope. The same SA sweep as LES is carried out in RANS, i.e. the SA is increased from KLSA by 2 CAD and reduced by 1 CAD. The resulting average in-cylinder pressure traces are reported in Figure 16 (right) for all the simulated spark times.
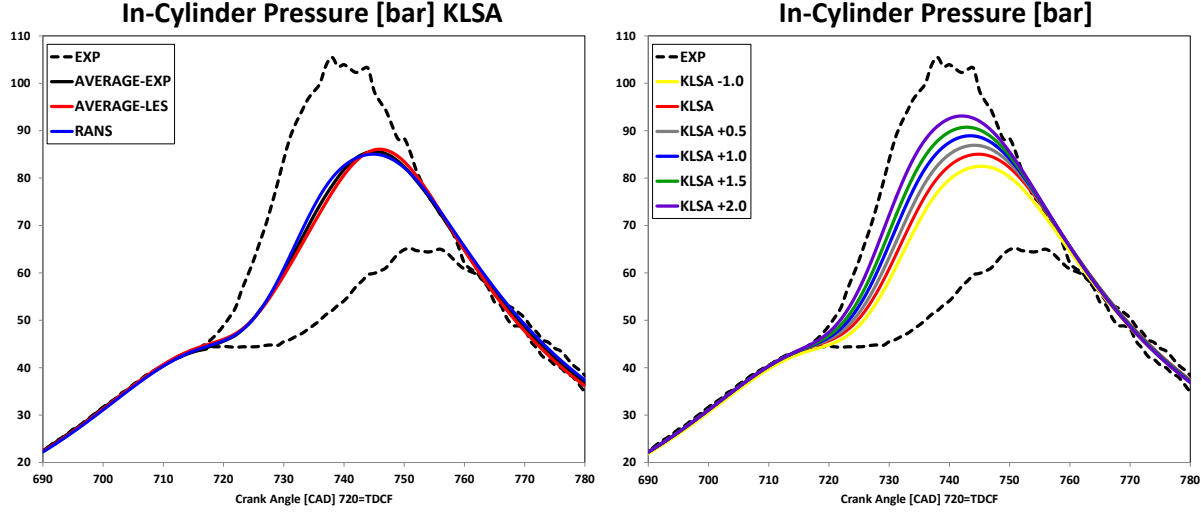

Figure 16: Average pressure traces: Comparison between RANS, LES and experiments at KLSA (left), and spark-sweep RANS results (right)

The HRR_{AI} is used to estimate the KI with the eMAPO function (Eq. 5), coherently with LES. The $eMAPO_{AVER}$ from RANS and LES are compared in Figure 17. Despite the same approach used to model knock in the two CFD frameworks, the average KI predicted by RANS is always lower than the LES derived one. This trend is systematic and it can be detected in all the simulated SA. However, this misalignment is explained discerning the average KI from the KI of the average cycle.
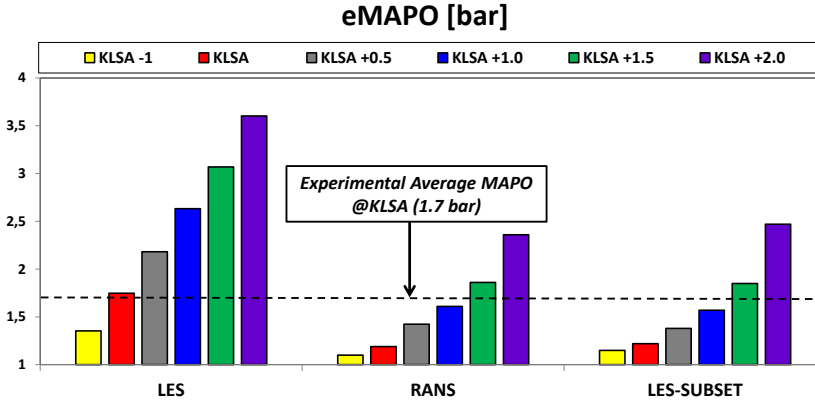

Figure 17. Average knock intensity (eMAPO) comparison between RANS and LES simulations changing the spark time.

Under soft knocking operations most of the cycles show a KI equal to the background noise, while combustion CCV causes sporadic cycles to exhibit high KI. A correlation is found in the experimental dataset between pressure peak and KI, i.e. high KI cycles are those showing the highest pressure peak, as shown in Figure 3. This is a consequence of the higher thermal loading of the end-gases, accelerating the mixture reactivity towards AI.

On the one hand, LES simulations account for combustion CCV and the resulting average KI is affected by the presence of both faster-than-average cycles (with high KI) and slower-than-average ones (almost null KI, not discernible from the combustion noise). Therefore, consistent observations are drawn on the average KI from LES and experiments. On the other hand, the same cannot be stated for RANS simulations. This is motivated by the intrinsic meaning of ensemble averaging in

the standard RANS formalism. Whereas the comparison of the experimental average pressure trace and the RANS result is formally correct, difficulties arise when analysing the KI. The reason for this is the lower limit for KI, i.e. slower-than-average cycles show a minimum KI equal to the background noise (lower bound for statistics), which in turn is equal to the one of the average pressure cycle (knock-free for KLSA). Conversely, KI statistics have no upper limitations and the average KI (from cycle-resolved analysis) is higher than the KI of the average cycle (from standard RANS). This motivates the need to discern the eMAPO$_{AVER}$ from the eMAPO of the average cycle.

To support the above considerations and verify the coherence of the two CFD datasets, the whole population of LES cycles (i.e. from all SA) are sub-divided into 6 different subsets based on their pressure peak value. In particular, for each SA, the LES cycles whose pressure peak is within ±0.5 bar from the pressure peak of the RANS cycle are clustered and the eMAPO$_{AVER}$ of each subset is calculated. The results of this procedure in terms of estimated KI are reported in Figure 17. If only LES cycles with similar peak pressures as the RANS cycles are considered, then the KI and eMAPO$_{AVER}$ of LES and the RANS are almost superimposed.

5. Statistical RANS-PDF results

The same engine operation of the presented RANS and LES analyses are finally simulated adopting the RANS-PDF knock model. As discussed above, the use of variance equations for enthalpy h_u and mixture fraction Z allows to predict different knocking events. In this case, the analysis is focused on low probability / high-KI events.
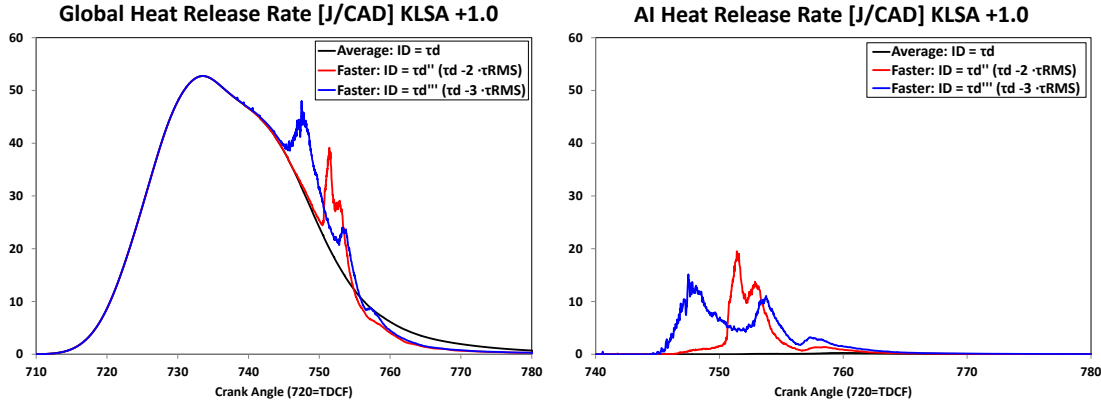
Figure 18: Global (left) and Auto-ignition (right) heat release rate using as source term for the integral knock precursor average and faster-than-average auto-ignition delay times.

Three different knocking events for each SA are simulated. Source terms for the Y_{IG} knock precursor (Eq. 2) the PDF-weighted AI delay (τ_d) and AI delays reduced by 2 and 3 standard deviations (τ_d'' and τ_d''', respectively), derived from Eq. 5 and 6, are in turn used. An example of the results of the RANS-PDF knock model is reported in Figure 18 for the KLSA+1.0 CAD case. As visible, three different knocking events are associated to the same combustion realization (i.e. same HRR before KO), i.e. the average one (in black) and two faster-than-average events (in red and blue lines). HRR$_{AI}$ is calculated by the combustion model in the same way in the same way as for the LES cases, and the resulting fraction of heat released by AI for the realizations considering τ_d'' and τ_d''' is illustrated in Figure 18 (right). Despite the KLSA+1.0 CAD operation, the average heat released by AI is negligible compared to the two faster-than-average realizations, reinforcing the poor meaning of knock detection from the ensemble average realization.

The fraction of heat released by AI (H$_{AI}$) is used to estimate the KI through the eMAPO function. The results are reported in Figure 19 for all the SA. The average KI (grey) does not overcome the MAPO$_{max}$=7 bar threshold in any of the simulated SAs, while the faster-than-average realizations (red and blue ones) exceed this limit for KLSA+0.5 CAD and furtherly advanced SA. In Figure 19 the estimated KI from the simulations with the RANS-PDF model are compared to the results from LES statistics in terms of average and maximum KI. The average KI underestimation is the same as in the standard model, while the τ_d''' realization is well representative of the maximum knock intensity. For KLSA+0.5 CAD operation the eMAPO''' reaches the 7 bar knock threshold, similarly to the maximum KI in both experiments and LES simulations.
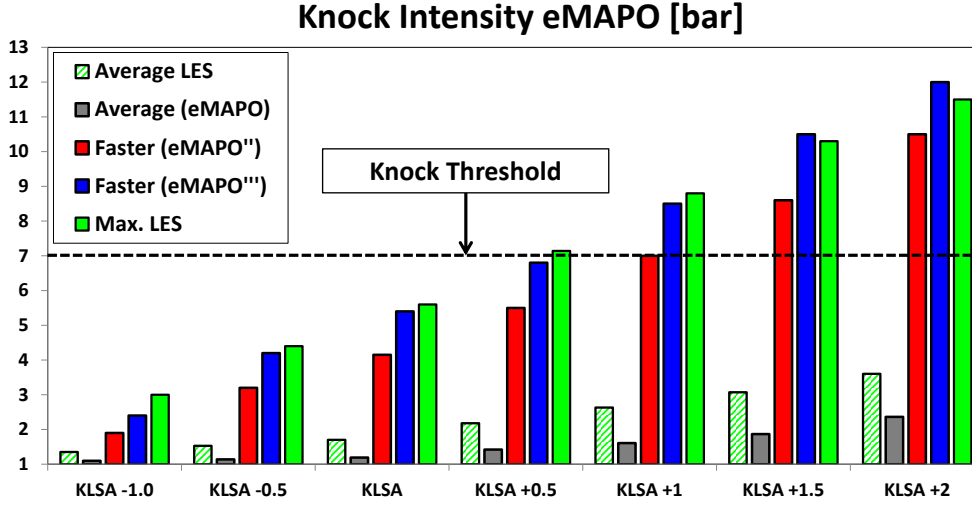
Figure 19: Knock Intensity (eMAPO) comparison between Statistical RANS and LES results changing the spark time. LES statistics (average and maximum KI) are reported in green bars.

Considering the average and the faster-than-average simulations, the KI variability is inferred as in Eq. 7-8. In particular, giving the two simulated faster-than-average realizations the standard deviation can be calculated as follows:

$$eMAPO''_{RMS} = (eMAPO'' - eMAPO_{AVER})/2 \qquad \text{Eq. 7}$$

$$eMAPO'''_{RMS} = (eMAPO''' - eMAPO_{aver})/3 \qquad \text{Eq. 8}$$

The resulting eMAPO$_{RMS}$ for all the simulated SA is reported in Figure 20 and compared to the LES-derived eMAPO$_{RMS}$, calculated as the standard deviation of the KI of the 23 simulated cycles. The eMAPO$_{RMS}$ predicted by the RANS-PDF model is comparable to the one from LES statistics for all SA, both in intensity and rate of increase. The analysed results show that an excellent agreement is found between the 3 RMS derived eMAPO$_{RMS}$ and the LES one.
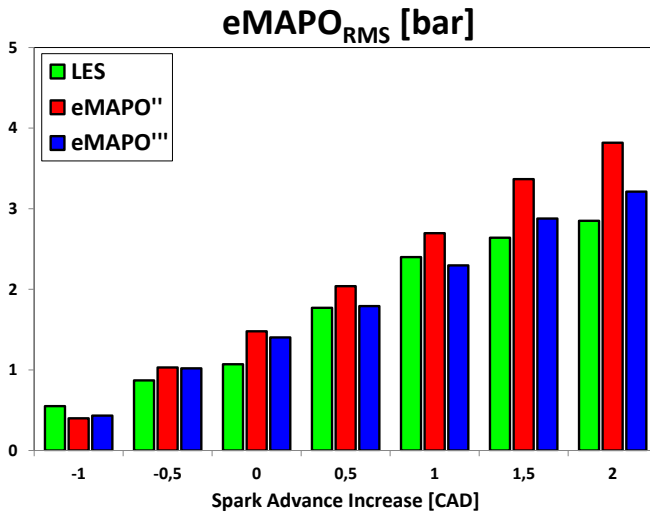
Figure 20: Comparison between LES knock intensity standard deviation (eMAPO$_{RMS}$) green bars and the statistical RANS derived one (blue and red bars) changing the spark time.

Log-normal distributions of KI are calculated from eMAPO$_{AVER}$ and eMAPO$_{RMS}$ and a fraction of knocking cycles (eMAPO>eMAPO$_{max}$) is inferred for increasingly advanced SA. In Figure 21 the comparison between the inferred knock probability from LES and RANS-PDF is reported, showing a good agreement between the two techniques. Both the

approaches are able to accurately predict the KLSA as the SA for which a 0.5 CAD advance would result in more than 1% of cycles overcoming the knock limit.
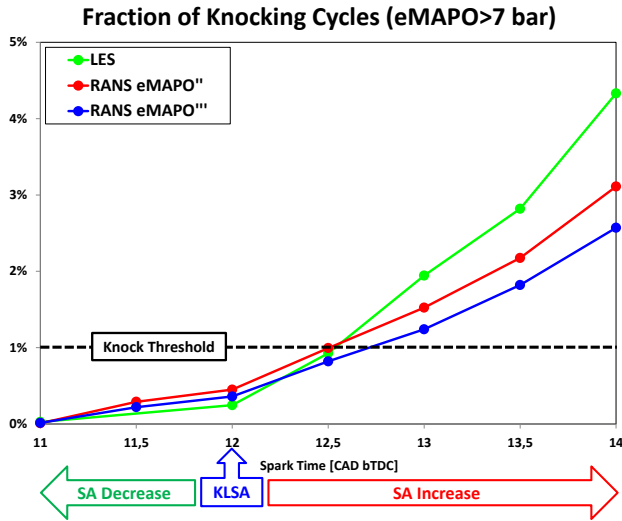
Fraction of Knocking Cycles (eMAPO>7 bar)

Figure 21: Estimated fraction of knocking cycles comparison between LES (green) and statistical RANS results (blue and red) changing the spark time.

As a consequence of the higher eMAPO$_{RMS}$, the fraction of knocking cycles predicted using the eMAPO'' indicator is higher than the one predicted through the eMAPO'''. Conversely, the knock frequency increase for advanced SA is underestimated by RANS despite the slight KI variability overestimation. This is motivated by the average KI underestimation. However, very similar results between all the approaches are obtained, and they confirm the applicability of the RANS-PDF model to small SA variations from the KLSA, which are most frequently tested operations.

Finally, the relevant difference in computational effort between RANS-PDF and LES is highlighted. On the one hand, 3 RANS cycles for initialization purposes followed by 25 cycles are simulated in LES to reach a reasonable convergence of statistics (2 of these discarded in order to be independent from the initial condition). On the other hand, just 3 cycles are calculated to reach cyclic convergence and to infer the knock probability with the RANS-PDF knock model. As the same grid was used in both models (i.e. no symmetry planes), the total CPU times are reported in Figure 22: the efficiency gain for the RANS-PDF model is evident, allowing to infer comparable knock statistics with a CPU cost more than 5 times lower. Finally, the use of symmetry planes could be introduced in RANS-PDF, leading to a further gain in CPU times and making it even more applicable in the industrial design framework.
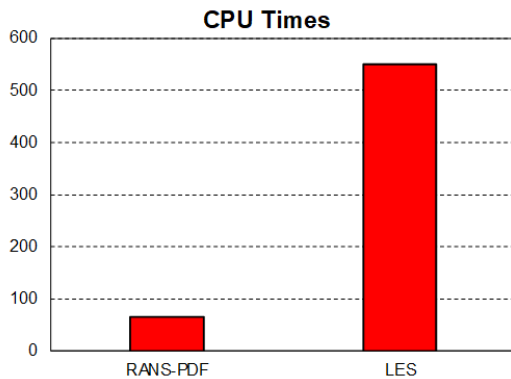

Figure 22: Comparison of CPU times between RANS-PDF (3 simulated cycles) and LES (25 simulated cycles).

6. Conclusions

Knock occurrence is one of the major barriers to the achievement of high thermal efficiency in turbocharged SI engines. Knock onset must be prevented to preserve the engine reliability, although the engine operating point should be as close as possible to knock onset to maximize the engine efficiency. The inherent stochastic nature of knock hinders its full characterization using ensemble averaged approaches. Knock occurrence can only be described through statistical indicators (e.g. percentiles). This is the case of engine testing, where the edge-of-knock operation is identified from knock statistics and not from the mean Knock Intensity (KI). This is motivated by the reduced engine durability caused by few high knocking events, which is poorly related to the average KI.

Accurate CFD models based on mechanisms for chemical kinetics of real fuel surrogates are used to predict knock onset and to understand the knock-responsible processes. Despite the stochastic character of knock would indicate LES as the appropriate modelling technique, the analysis is usually carried out in a standard RANS framework (i.e. accounting only for the ensemble average realization for both flame propagation and end-gas reaction rate). The different meaning of the average KI from the KI of the average cycle is the origin of the underestimation of the simulated KI in standard RANS simulations. In the current study the full power high-speed operation of a currently made GDI engine is simulated using the following approaches:

- Multi-cycle LES simulations are carried out, in order to generate a background of cycle-resolved knock simulation. Converged statistics of the LES results are at first demonstrated. Log-normal distributions are then calculated based on the LES dataset, and the KLSA is indicated following the same procedure used at the test bench, i.e. the maximum SA with less 1% of cycles exceeding a predefined KI limit. Despite a statistically reduced number of engine cycles (23), the convergence of combustion and knock statistics allows to meet a good agreement between experiments and CFD. LES is able to accurately predict the edge-of-knock operation (i.e. KLSA) following the same statistical analysis adopted in the experiments and using as knock index the eMAPO function, considering a 1.1 bar combustion noise. LES results well reproduce the experimental outcomes in terms of average values and variability of both combustion and knock, thus confirming the reliability of the developed CFD methodology.
- The spark time is virtually advanced in CFD with a step of 0.5 CAD, moving the engine operation from edge-of-knock into knocking conditions. LES results are used to infer the rate of increase of knock probability for advanced SAs. LES simulations serve as virtual experiments for conditions in which the engine cannot be tested for durability requirements. Log-normal functions are used to presume a fraction of knocking cycles for SA variation.
- The same engine conditions are simulated in a RANS framework: the resulting average KI for each SA is compared to the LES one. Despite the same approach is used to predict end-gas reactivity, RANS results suffer from a systematic underestimation of KI compared to LES results. This is motivated by a substantial difference between the average KI (calculated from statistics of experiments or LES) and the KI of the ensemble average cycle (from standard RANS). As a consequence, standard RANS can only provide average KI while no information on knock probability can be inferred. This poses difficulties in identifying the KLSA using RANS.
- An improved RANS-PDF knock model developed by the authors is finally adopted to overcome the previously described RANS limitations. The model relies on transport equations for variance of mixture fraction (Z) and enthalpy (h_u), from which the unburnt temperature T_u is obtained. It allows to infer a fraction of knocking cycles for each SA based on local turbulence and gradients, thus covering the gap between LES and traditional RANS. In addition to the average KI (as standard RANS), the deviation from the average KI is inferred (e.g. earlier-than-average knocking cycles). The comparison with knock probability is in good agreement with the LES-derived one for all the SA, and very similar log-normal distribution functions of knock tendency result from the RANS-PDF knock model.

The presented results show that the developed RANS-PDF knock model can provide a knock indication based on statistical analysis, thus making it straightforwardly comparable to test bench outcomes. The proposed model relevantly enriches the meaning of RANS-derived knock results, poorly representative when limited to ensemble average knock only. The obtained knock statistics from the RANS-PDF model are compared to those obtained using multi-cycle LES simulations, and results are in good agreement in terms of tendency (e.g. predicted fraction of knocking cycles). This indicates the RANS-PDF knock model as an excellent trade-off between CPU cost and result accuracy when dealing with knock statistics, which can be easily integrated in the RANS-based industrial design workflow. The innovative analysis capabilities given by the RANS-PDF model substantially expand the understanding of the knock-inceptor phenomena in highly boosted SI engines and allow a coherent and quantitative comparison between simulations and experiments.

References

[1] Kufferath, I. A., Naber, D. I. D., Mailänder, D. I. E., & Maier, I. R. (2018). The Path to a Negligible NO2 Immission Contribution from the Diesel Powertrain. In 39 th International Vienna Motor Symposium.

[2] Di Blasio, G., Beatrice, C., Belgiorno, G., Pesce, F. et al., "Functional Requirements to Exceed the 100 kW/l Milestone for High Power Density Automotive Diesel Engines," SAE Int. J. Engines 10(5):2342-2353, 2017, https://doi.org/10.4271/2017-24-0072.

[3] International Energy Agency, World Energy Outlook 2017. Available online at https://www.eia.gov/outlooks/ieo/pdf/0484(2017).pdf

[4] Wang Z., Liu H., Reitz R. D., "Knocking combustion in spark-ignition engines", Progress in Energy and Combustion Science, 61 (2017) pp. 78-112

[5] Zhen X., Wang Y., Xu S., Zhu Y., Tao C., Xu T., Song M., "The engine knock analysis – An Overview", Applied Energy, 92(2012), pp. 628-636

[6] Alagumalai, "Internal Combustion engines: Progress and prospects", Renewable and Sustainable Energy Reviews, 38, (2014) pp. 561-571

[7] Attard W., Toulson E., Watson H., Hamori F., "Abnormal Combustion Including Mega Knock in a 60% Downsized Highly Turbocharged PFI Engine", SAE Techical Paper 2010-01-1456 (2010)

[8] Turner J., Popplewell A., Pattel R., Johnson T., "Ultra Boost for Economy: Extending the limits of extreme engine Downsizing", SAE International Journal of Engines, 7(1), (2014) pp. 387-417

[9] Heywood J., "Internal Combustion Engines Fundamentals", New York: McGraw-Hill Education, 1988

[10] Wang Z., Wang Y., Reitz R.D., "Pressure oscillation and chemical kinetics coupling during knock processes in gasoline engine combustion", Energy & Fuels, 26 (12), (2012) pp. 7107-19

[11] Kalghatgi G., "Developments in internal combustion engines and implication for combustion science and future transport fuel", Proceeding of Combustion Institute, 35 (1), (2015) pp. 101-115

[12] Kalghatgi G., Bradley D., "Pre-Ignition and 'super knock' in turbo-charged spark ignition engines", International Journal of Engine Research, 13 (2012) pp. 399-414

[13] Severi E., d'Adamo A., Berni F., "Numerical investigation on the effects of bore reduction in a high performance turbocharged GDI engine. 3D investigation of knock tendency", Energy Procedia, 81(2015), pp. 846-855

[14] Kalghatgi GT., "Fuel anti-knock quality –part 2. Vehicle studies – How relevant is motor octane number MON in current engines?", SAE Technical Paper, 2001-01-3585, (2001)

[15] Kalghatgi, G., Nakata, K., and Mogi, K., "Octane Appetite Studies in Direct Injection Spark Ignition (DISI) Engines," SAE Technical Paper 2005-01-0244, 2005, https://doi.org/10.4271/2005-01-0244.

[16] Wei H., Feng G., Pan M., et al., "Experimental investigation on the knocking combustion characteristics of n-butanol gasoline blends in a DISI engine", Applied Energy, 175(2016), pp. 346-355,

[17] Merola S., Valentino G., Tornatore C., Marchitto L., "In-cylinder spectroscopic measurements of knocking combustion in a SI engine fueled with butanol-gasoline blend", Energy, 62(2013), pp.150-161

[18] Berni F., Breda S., d'Adamo A., Fontanesi S., "Numerical Investigation on the Effects of Water/Methanol Injection as Knock Suppressor to Increase the Fuel Efficiency of a Highly Downsized GDI Engine", SAE Technical Paper, 2015-24-2499

[19] Abu-Qudais M., "Exhaust gas temperature for knock detection and control in spark ignition engine", Energy and Conversion Management, 37 (1996) pp. 1383-1392

[20] Vafamehr H., Cairns A., Sampson O., et al., "The competing chemical and physical effects of transient fuel enrichment on heavy knock in an optical spark ignition engine", Applied Energy, 179(2016), pp. 687-697

[21] d'Adamo A., Berni F., Breda S., "A Numerical investigation on the potentials of Water Injection as a Fuel Efficiency enhancer in Highly Downsized GDI engines", SAE Technical Paper, 2015-01-0393

[22] Berni F., Breda S., Lugli M., Cantore G., et al., "A numerical investigation on the potentials of water injection to increase knock resistance and reduce fuel consumption in highly downsized GDI engines", Energy Procedia, 81(2015), pp. 826-835

[23] Lanzafame R., "Water Injection effects on a single-cylinder CFR engine", SAE Technical Paper, 1999-01-0568

[24] Battistoni, M., Grimaldi, C., Cruccolini, V., Discepoli, G. et al., "Assessment of Port Water Injection Strategies to Control Knock in a GDI Engine through Multi-Cycle CFD Simulations," SAE Technical Paper 2017-24-0034, 2017.

[25] Liu H., Wang Z., Long Y., Wang J., "Dual Fuel Spark Ignition (DFSI) combustion fuelled with different alcohols and gasoline for fuel efficiency", Fuel, 157 (2015), pp. 255-260

[26] Liu H., Wang Z., Wanf J., "Methanol-gasoline DFSI (Dual Fuel Spark Ignition) combustion with dual-injection for engine knock suppression", Energy, 73 (2014), pp. 686-693

[27] Breda S., Berni F., d'Adamo A., et al., "Effects on knock intensity and specific fuel consumption of port water/methanol injection in a turbocharged GDI engine: Comparative analysis", Energy Procedia, 82(2015), pp. 96-102

[28] Alger T., Mangold B., Roberts C., Gingrich J., "The interaction of fuel anti-knock index and cooled EGR on engine performance and efficiency", SAE International Journal of Engines, 5 (2015), pp. 1229-1241

[29] Bozza F., De Bellis V., Teodosio L., "Potentials of cooled EGR and water injection for knock resistance and fuel consuption improvements of gasoline engines", Applied Energy, 169(2016), pp. 112-125

[30] Peters N., Kerschgens B., Paczko G., "Super-knock prediction using a refined theory of turbulence", SAE International Journal of Engines, 6 (2013) pp. 953-96

[31] Luisi S., Doria V., Stroppiana A., Millo F., Mirzaeian M., "Experimental investigation on early and late intake valve closures for knock mitigation through Miller cycle in a downsized turbocharged engine", SAE Technical Paper , 2015-01-0760

[32] Teodosio L., Pirrello D., Berni F., et al., "Impact of intake valve strategies on fuel consumption and knock tendency of a spark ignition engine", Applied Energy, 216(2018), pp. 91-104

[33] Spelina J. M., Peyton Jones J. C., Frey J., "Characterization of knock Intensity distributions: Part 1: statistical independence and scalar measures", Proceedings of the Institution of Mechanical Engineers, Part D: Journal of automobile Engineering, 228(2) 2014 pp. 117-128

[34] Spelina J. M., Peyton Jones J. C., Frey J., "Characterization of knock Intensity distributions: Part 2: parametric models", Proceedings of the Institution of Mechanical Engineers, Part D: Journal of automobile Engineering, 227(12) 2013

[35] D'Adamo, A., Breda, S., Fontanesi, S., and Cantore, G., "A RANS-Based CFD Model to Predict the Statistical Occurrence of Knock in Spark-Ignition Engines," SAE Int. J. Engines 9(1):618-630, 2016, https://doi.org/10.4271/2016-01-0581.

[36] d'Adamo A., Breda S., Fontanesi S., Irimescu A., "A RANS knock model to predict the statistical occurrence of engine knock", Applied Energy, 191(2017), pp. 251-263

[37] d'Adamo A., Breda S., Iaccarino S., Berni F., et al., "Development of a RANS-Based Knock Model to Infer the Knock Probability in a Research Spark-Ignition Engine", SAE International Journal of Engine, 10(3), (2017) pp. 722-739

[38] Vancoillie J., Sileghem L., Verhelst S., "Development and validation of a quasi-dimensional model for methanol and ethanol fueled SI engines", Applied Energy, 132 (2014) pp.412-425

[39] Breda S., d'Adamo A., Fontanesi S., et al., "CFD Analysis of Combustion and Knock in an Optically Accessible GDI Engine", SAE International Journal of Engines, 9(1), (2016) pp. 641-656

[40] Iaccarino, S., Breda, S., D'Adamo, A., Fontanesi, S. et al., "Numerical Simulation and Flame Analysis of Combustion and Knock in a DISI Optically Accessible Research Engine," SAE Int. J. Engines 10(2):576-592, 2017

[41] d'Adamo A., Breda S., Cantore G., "Large-eddy simulation of cycle-resolved knock in a turbocharged SI engine", Energy Procedia, 82(2015), pp. 45-50

[42] d'Adamo, A., "Numerical Investigation of Abnormal Combustion and Knock in High-Performance S.I. Engines," PhD Thesis 2015, University of Modena and Reggio Emilia, DOI: 10.13140/RG.2.1.1159.2405

[43] Robert A., Richard S., Colin O., Poinsot T., "LES study of deflagration to detonation mechanism in a downsized spark ignition engine", Combustion and Flame, 162(7), (2015) pp. 2788-2807

[44] Robert A., Richard S., Colin O., Martinez L., De Francqueville L., "LES prediction and analysis of knocking combustion in a spark ignition engine", Proceedings of the Combustion Institute, 35 (2015) pp. 2941-2948

[45] Misdariis A., Vermorel O., Poinsot T., "LES of knocking in engines using dual heat transfer and two-step reduced schemes", Combustion and Flame, 162 (2015) pp. 4304-4312

[46] Linse D., Kleemann A., Hasse C., "Probability density function approach coupled with detailed chemical kinetics for the prediction of knock in turbocharged direct injection spark ignition engines", Combustion and Flame, 161 (2014), pp.997-1014

[47] Fontanesi S., Paltrinieri S., and Cantore G., "LES analysis of cyclic variability in GDI engine", SAE technical paper 2014-01-1148

[48] Fontanesi S., Paltrinieri S., Tiberi A., d'Adamo A., "LES multi-cycle analysis of a high performance GDI engine" SAE technical paper 2013-01-1080

[49] Fontanesi S., Paltrinieri S., d'Adamo A., Duranti S., "Investigation of boundary condition effects on the analysis of cycle-to-cycle variability of a turbocharged GDI engine", Oil and Gas Science Technology – Rev IFP Energies nouvelles 69(1), (2014) pp. 107–128

[50] Berni, F., Cicalese, G., Fontanesi, S., "A modified thermal wall function for the estimation of gas-to-wall heat fluxes in CFD in-cylinder simulations of high performance spark-ignition engines," Applied Thermal Engineering Volume 115, 25 March 2017, Pages 1045-1062

[51] Cicalese, G., Berni, F., and Fontanesi, S., "Integrated In-Cylinder / CHT Methodology for the Simulation of the Engine Thermal Field: An Application to High Performance Turbocharged DISI Engines," SAE Int. J. Engines 9(1):601-617, 2016.

[52] Smagorinsky J., "General circulation experiments with the primitive equations", Mon Wea Rev 1963; 91: 99–164.

[53] Postrioti, L., Cavicchi, A., Brizi, G., Berni, F. et al., "Experimental and Numerical Analysis of Spray Evolution, Hydraulics and Atomization for a 60 MPa Injection Pressure GDI System," SAE Technical Paper 2018-01-0271, 2018, https://doi.org/10.4271/2018-01-0271.

[54] Reitz R., Diwakar R., "Effect of drop breakup on fuel sprays" SAE paper 860469, SAE Trans 1986; 95(3):218–227.

[55] Colin, O., Benkenida, A., "The 3-Zones Extended Coherent Flame Model (ECFM3Z) for Computing Premixed/Diffusion Combustion," Oil & Gas Science and Technology – Rev. IFP, 59(6), (2004), pp. 593-609

[56] Vermorel O., Richard S., Colin O., Angelberger C., Benkenida A., and Veynante D., "Towards the understanding of cyclic variability in a spark ignited engine using multicycle LES" Combustion and Flame 156 (2009) pp. 1525–1541

[57] d'Adamo, A., Del Pecchia, M., Breda, S., Berni, F. et al., "Chemistry-Based Laminar Flame Speed Correlations for a Wide Range of Engine Conditions for Iso-Octane, n-Heptane, Toluene and Gasoline Surrogate Fuels," SAE Technical Paper 2017-01-2190, 2017, https://doi.org/10.4271/2017-01-2190.

[58] Breda, S., d'Adamo, A., Fontanesi, S., D'Orrico, F. et al., "Numerical Simulation of Gasoline and n-Butanol Combustion in an Optically Accessible Research Engine," SAE Int. J. Fuels Lubr. 10(1):32-55, 2017, https://doi.org/10.4271/2017-01-0546

[59] Del Pecchia, M., Breda, S., D'Adamo, A., Fontanesi, S. et al., "Chemistry-Based Laminar Flame Speed Correlation for Part-Load SI Conditions and Validation in a GDI Research Engine," SAE Int. J. Engines 11(6):2018, https://doi.org/10.4271/2018-01-0174.

[60] Boudier P., Henriot S., Poinsot T., Baritaud T., "A Model for Turbulent Flame Ignition and Propagation in Spark Ignition Engines," Twenty-Fourth Symposium (International) on Combustion/The Combustion Institute, 1992 pp. 503-510.

[61] Colin O., Truffin K., "A spark ignition model for Large Eddy Simulation based on FSD transport equation (ISSIM-LES)", Proceedings of the Combustion Institute, 33 (2011), pp. 3097-3104

[62] d'Adamo A., Breda S., Fontanesi S., Cantore G., "LES Modelling of Spark-Ignition Cycle-to-Cycle Variability on a Highly Downsized DISI Engine," SAE International Journal of Engines 8(5), (2015) pp. 2029-2041

[63] d'Adamo, A., Breda, S., Berni, F., and Fontanesi, S., "Understanding the Origin of Cycle-to-Cycle Variation Using Large-Eddy Simulation: Similarities and Differences between a Homogeneous Low-Revving Speed Research Engine and a Production DI Turbocharged Engine," SAE Int. J. Engines 12(1):2019.

[64] Andrae J. C. G., Head R. A., "HCCI Experiments with gasoline surrogate fuels modeled by a semidetailed chemical kinetic model", Combustion and Flame, 156 (2009) pp. 842-851

[65] Morgan, N., Smallbone, A., Bhave, A., Kraft, M., Cracknell, R., Kalghatgi, G., "Mapping surrogate gasoline compositions into RON/MON space," Combustion and Flame Volume 157, Issue 6, June 2010, Pages 1122-1131

[66] Lafossas F., Castagne M., Dumas J., Henriot S., "Development and Validation of a Knock Model in Spark Ignition Engines using a CFD code", SAE Technical Paper, 2002-01-2701

[67] Fox, R. O., Computational models for turbulent reacting flows, Cambridge University Press, 2000.

[68] Klimstra, J., "The Knock Severity Index – A Proposal for a Knock Classification Method," SAE Technical Paper 841335

Nomenclature

|	
AI	Auto-ignition
BC	Boundary Condition
CCV	Cycle-to-Cycle Variability
CDF	Cumulative Density Function
CFL	Courant–Friedrichs–Lewy
CoV	Coefficient of Variation
DI	Direct Injection
eMAPO	Estimated Maximum Amplitude of Pressure Oscillation
eMAPO$_{AVER}$	eMAPO calculated based on the PDF-averaged $\tilde{\tau}_d$
eMAPO$_{RMS}$	Standard deviation of eMAPO
FSD	Flame Surface Density
HRR	Heat Release Rate
ISSIM	Imposed Stretch Spark Ignition Model
KI	Knock Intensity
KLSA	Knock Limited Spark Advance
KO	Knock Onset
KSI	Knock Severity Index
IC	Initial Condition
ICE	Internal Combustion Engine
LES	Large-Eddy Simulation
LFS	Laminar Flame Speed
LIVC	Late Intake Valve Closing
LUT	Look-Up Table
MAPO	Maximum Amplitude of Pressure Oscillation
MAPO$_{max}$	Maximum MAPO threshold for the 1% fraction of highest knocking cycles
PDF	Probability Density Function
RANS	Reynolds-Average Navier-Stokes
RANS-PDF	RANS equations with the addition of transport equations for variances
SA	Spark Advance
SI	Spark Ignition
TRF	Toluene Reference Fuel

Appendix 1
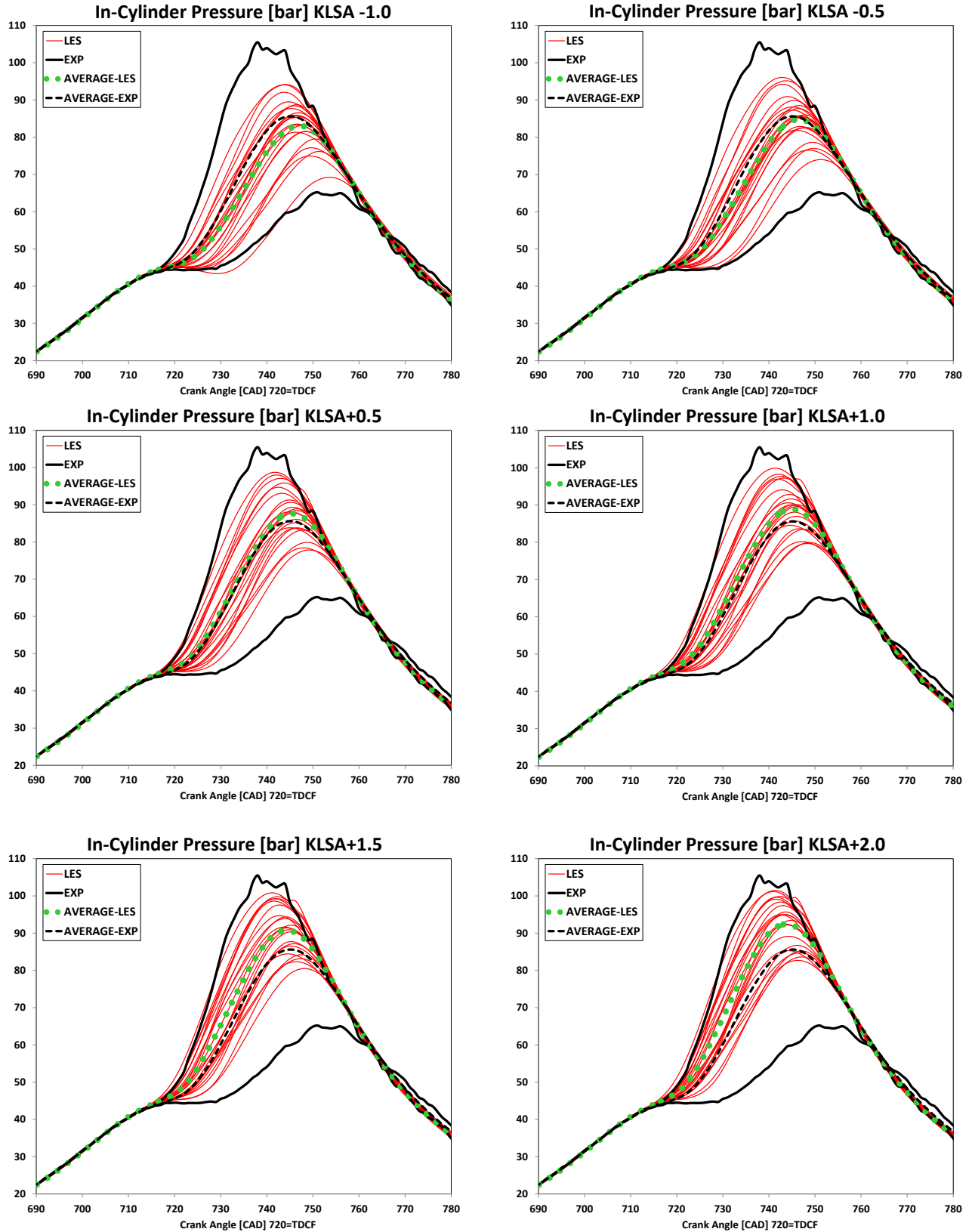
Figure A1: In-cylinder pressure traces of the 23 considered cycle LES for all the simulated spark times